IEEE Photonics Journal
An IEEE Photonics Society Publication

Optimal Transmission of VLC System in the Presence of LED Nonlinearity and APD Module Saturation

Volume 10, Number 5, September 2018

Meijun Gao
Chao Li
Zhengyuan Xu, ***Senior Member, IEEE***

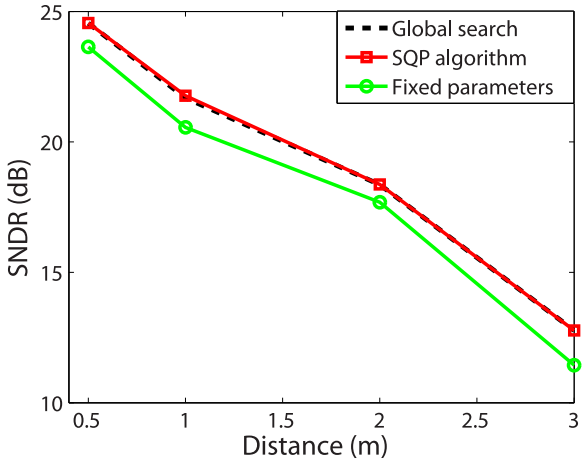

DOI: 10.1109/JPHOT.2018.2871148
1943-0655 © 2018 IEEE

IEEE photonics SOCIETY

IEEE

Optimal Transmission of VLC System in the Presence of LED Nonlinearity and APD Module Saturation

Meijun Gao,[1] **Chao Li**,[1]
and Zhengyuan Xu,[1,2] ***Senior Member, IEEE***

[1]Key Laboratory of Wireless-Optical Communications, Chinese Academy of Sciences, University of Science and Technology of China, Hefei 230026, China
[2]Shenzhen Graduate School, Tsinghua University, Shenzhen 518055, China

DOI:10.1109/JPHOT.2018.2871148

Manuscript received July 19, 2018; accepted September 14, 2018. Date of publication September 24, 2018; date of current version October 9, 2018. This work was supported in part by the Anhui Provincial Natural Science Foundation under Grant 1808085MF186, in part by the Key Program of National Natural Science Foundation of China under Grant 61631018, and in part by the Key Research Program of Frontier Sciences of CAS under Grant QYZDY-SSW-JSC003. Corresponding author: Chao Li (e-mail: cli0620@ustc.edu.cn).

Abstract: We address the optimal transmission of LED-based visible light communication (VLC) system using direct current biased optical orthogonal frequency division multiplexing (DCO-OFDM) modulation and avalanche photodiode (APD) receiver. The peak-to-average-power ratio (PAPR) characteristic of O-OFDM signal is studied, which reveals that the careful setting of transmission parameters is necessary for O-OFDM signal with high PAPR to avoid the severe nonlinear distortion. We further experimentally investigate the nonlinear distortion caused by the LED clipping and APD module saturation, and define a modified term called signal-to-noise and distortion ratio (SNDR) to measure the influence of nonlinear distortion on system performance. The derived explicit expression of SNDR shows that the performance depends on the transmission parameters of both direct current bias V_{dc} and peak-to-peak voltage V_{pp}. Meanwhile the sequential quadratic programming algorithm is applied to maximize SNDR and obtain the optimal transmission parameters. The optimal transmission of the nonlinear LED-VLC system is achieved via both simulations and experiments.

Index Terms: Visible light communication (VLC), optical orthogonal frequency division multiplexing (O-OFDM), light-emitting diode (LED) nonlinearity, avalanche photodiode (APD) module saturation, signal-to-noise and distortion ratio (SNDR) optimization.

1. Introduction

Recently, the indoor visible light communication (VLC) using light-emitting diode (LED) source has drawn high attention from both academia and industrial areas, due to the development of LED technology for indoor solid-state lighting and the potential for wireless data transmission simultaneously [1]. The LEDs are widely employed as lighting sources because of their long life expectancy, low power consumption, and low cost. Meanwhile the transmitted signal can be modulated onto the LED without causing flicker perceived by the human eyes. In order to obtain the data sent from LEDs, photoelectric converter, such as avalanche photodiode (APD) that has higher gain than photo diode (PD) [2], is used to convert the light signal into electrical signal at the receiver.

Usually, the commercial LEDs have several MHz of 3 dB-modulation bandwidth. To enhance the transmission capacity of LED-VLC systems, orthogonal frequency division multiplexing (OFDM) modulation can be used due to its high spectral efficiency (SE) [3], [4]. In an intensity-modulation direct-detection (IM/DD) LED-VLC system, the time-domain electrical signal used to drive the LED must be real and non-negative. The real-valued signal in optical OFDM (O-OFDM) requires the input data on OFDM subcarriers to be Hermitian symmetry (HS). There are two main schemes to satisfy the non-negative requirement of signal in O-OFDM. One is the addition of a DC bias, known as DCO-OFDM [5]. The other scheme, known as asymmetric clipping optical OFDM (ACO-OFDM) [6], is to clip the negative part of the time-domain signal and only transmit the positive part. In order to ensure the complete recovery of original signal from the clipped signal with only the positive part, only odd subcarriers are used to transmit data symbols in ACO-OFDM, resulting in the loss of half SE. Hence, DCO-OFDM, which carries the transmitted data at all subcarriers, has double SE compared with ACO-OFDM [7]. Taking into account the limited modulation bandwidth of commercial LEDs, we employ DCO-OFDM in this work.

In the practical VLC system, the nonlinear characteristics of LED and the APD module deteriorate the system performance greatly, especially for the OFDM signal. On the one hand, due to the nonlinear electrical-to-optical conversion (EOC) of LED, the driving signal is clipped once it's outside the limited linear region of LED. Hence the peak values of driving signal should be within the limited linear region of LED to avoid the clipping distortion. However, it's well known that the O-OFDM signal has larger peak-to-average-power ration (PAPR) than the single-carrier modulation, which means that the driving signal is prone to be clipped and distorted excessively in our DCO-OFDM VLC system. On the other hand, the avalanche effect and large gain of APD module make it easier to be saturated than PD, which results in the signal distortion and thus system performance deterioration once the received optical power (ROP) is overlarge. As far as we all know, the response of APD under different ROP, especially the influence of APD module saturation, has not been considered in the indoor VLC system.

To develop a LED-VLC system, the transmission parameters, including the peak-to-peak value V_{pp} and the direct current (DC) bias V_{dc}, should be set before the data transmission. The electrical power of the transmitted alternate current (AC) electrical signal is proportional to the square of V_{pp}. If V_{pp} is too small, the signal power is insufficient to support the long distance transmission, while the large V_{pp} will lead to LED clipping and thus introduce severe clipping noise. The DC bias needs to be coupled into the electrical AC signals to drive the LED and turn the DCO-OFDM signals into non-negative ones. If the V_{dc} is too small, some negative parts of the signals may be clipped due to the non-negative constraint of the signal used to drive LED. If the V_{dc} is too large, the upper peak of the AC signals will also be clipped. Moreover, note that V_{dc} greatly determines the ROP at the receiver side and the response of APD module. Therefore, the transmission parameters influence not only the power of the transmitted signals and the degree of the signals to be clipped, but also the response of APD module. The reasonable setting of transmission parameters is essential to improve the performance of the system, especially in the O-OFDM system with inherent high PAPR.

In this paper, we first study the PAPR characteristic of the electrical OFDM signal with HS (we called it O-OFDM). It is found that O-OFDM has higher PAPR than that of traditional radio frequency (RF) OFDM due to its HS structure, which contradicts the limited linear range of LED. Furthermore, we experimentally investigate the nonlinearity of the LED source and saturation characteristic of APD module, which jointly affect the system performance. For that reason, the signal-to-noise and distortion ratio (SNDR) is defined to measure the influence of distortions caused by both the clipping of LED and APD module saturation on the performance of the system. The analytic expression of SNDR based on the characteristics of LED and APD module and linked with the transmission parameters V_{pp} and V_{dc} is obtained. The optimal transmission parameters could be found by maximizing SNDR, which is a complex non-convex optimization problem. The sequential quadratic programming (SQP) algorithm is applied to solve this problem and obtain the optimal transmission parameters accurately and efficiently. The theoretical analysis of the nonlinear VLC system and the performance of the algorithm are verified by both simulations and experimental

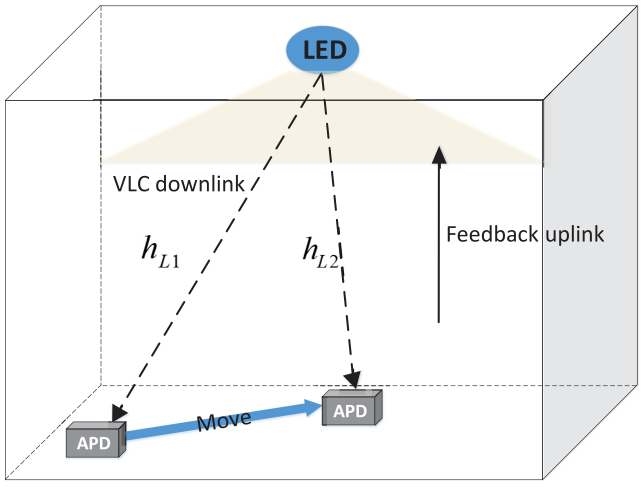

Fig. 1. A classic point-to-point indoo LED-VLC system using APD module with mobile user and feedback link.

results. Once the channel of the user changes, the optimal transmission performance can still be realized rapidly according to our simulations.

2. System Problem Statement

2.1 Scenario Description

Consider a classic indoor VLC system with a single LED and a single mobile user, as depicted in Fig. 1. The LED is employed as the transmitter, which is fixed on the center of the ceiling. The mobile user equipped with APD as the receiver can move to any place of the horizontal receiver plane. In this system, the transmission parameters, V_{dc} and V_{pp}, need to be determined by the transmitter to achieve good system performance. Due to the mobility of the user, the optimal transmission parameters need to be updated once the channel changes. In addition to a VLC downlink for data transmission, there is also a reliable uplink used for feeding back some necessary information to assist in updating the transmission parameters at the LED transmitter. Note that the uplink feedback channel can be realized by the technology of VLC, infra-red communication or RF communication. In the following sections, the characteristics of LED nonlinearity and APD module saturation and the inherent high PAPR of the O-OFDM are investigated in detail, which reveals that the system performance is limited by the nonlinearities of devices and signal characteristics. Hence, the proper choice of transmission parameters is crucial for the LED-VLC systems.

2.2 Characteristics of LED Nonlinearity and APD Module Saturation

Like most VLC systems in [8], [9], [10], LED is a nonlinear device, and modulated in a voltage-driven manner, where the desired signal with time-varying voltage is added to the DC bias. The P-V characteristic of a commercial LED employed as the front-end transmitter in our VLC system is shown in Fig. 2(a), where the experimental data, the polynomial fitting curve with five order and the piece-wise linear fitting curve are included. The measured experimental data shows that the output optical power is linearly correlative to the input voltage that locates between 2.7 V and 4.5 V. Furthermore, the input signal used to drive the LED is clipped when its instantaneous voltage is outside the linear region. It's seen that the turn-on voltage required to light on the adopted LED is 2.7 V. Since too large voltage/current may significantly shorten the LED life time, a voltage/current-limit circuit is usually implemented to limit the maximum permissible voltage/current of the transmitted signal [9], [10]. The maximum input voltage of the adopted LED is set to 4.5 V.

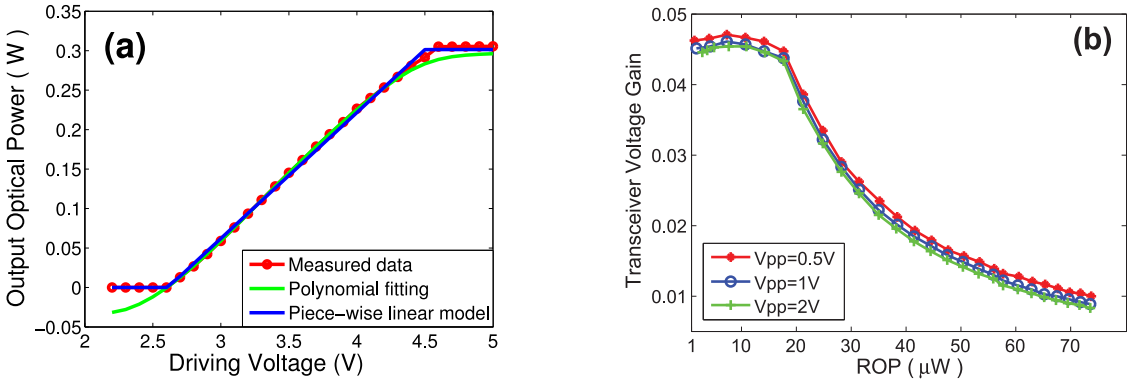

Fig. 2. Characteristics of deveices. (a) LED P-V curves. (b) Transceiver voltage gain of APD module as the function of ROP.

Compared with the 5-order polynomial model, the piece-wise linear model composed of the turn-on voltage U_b of 2.7 V as well as the maximum voltage U_t of 4.5 V is more simpler and convenient for following analysis. Furthermore, it's obvious that the piece-wise linear model fits better than the polynomial model, especially at the clipped area. Due to its simplicity and well-fitting characteristic, the piece-wise linear model is adopted in this paper, where the slope term $k = 0.1595$ and the intercept $b = 0.4165$. Note that even if the LED is modulated in a current-driven manner, the nonlinear characteristic and the LED clipping still limit the system performance due to the turn-on current and the maximum permissible current. The turn-on current corresponding to the turn-on voltage in Fig. 2(a) defines the minimum current to light the LED. As mentioned before, the maximum permissible current corresponding to the maximum voltage is limited to protect the LED device. Hence the input signal used to drive LED will be clipped when it's above the maximum permissible current or below the turn-on current. Furthermore, the proposed piece-wise linear model may still fit well the clipping characteristic of LED driven by current.

The APD module is composed of an optical-to-electrical convertor (OEC) with responsivity of R and the following TIA with gain of g. As far as we know, the conversion gain $R \times g$ (unit: V/W) is always assumed to be a constant in the existing literatures. However, the experiment measurements show that the APD module will saturate when ROP is large enough, and then the conversion gain decreases, which means that the real conversion gain varies with ROP.

Recall that a time-varying signal is added to the constant bias to drive the LED in the voltage-driven modulation. The transmitted electrical signal includes the zero-mean AC signal component and the constant DC bias. Assuming that the modulation is performed in the linear regime of LED, the transmitted optical signal comprises of the zero-mean AC signal component and the constant power bias, respectively. Let P_{DC_Tx} denote the constant optical power bias, and P_{AC_Tx} denote the optical power of the zero-mean optical AC signal. For APD module at the receiver side, ROP is the optical power of the received optical signal, which includes the received DC bias and the received AC signal component. Let P_{DC_Rx} and P_{AC_Rx} denote the optical power of the received optical DC and AC components, respectively. Note that P_{DC_Rx} and P_{AC_Rx} are the attenuations of P_{DC_Tx} and P_{AC_Tx}, respectively, due to the optical link loss. Although the whole ROP affects the responsivity of APD module, the output voltage of APD module depends only on P_{AC_Rx}, since APD module blocks the DC optical signal. In practice, it's hard to measure the power P_{AC_Rx} as well as the conversion gain because the optical AC power mixed with the DC component cannot be separated before the APD receiver. Therefore, we define the transceiver voltage gain G to investigate the influence of ROP on the conversion gain of APD module. Specifically, $G \triangleq \frac{V_{AC\_Rx}}{V_{AC\_Tx}}$, where V_{AC_Rx} and V_{AC_Tx} denote the amplitudes of AC electrical signals at the receiver and transmitter sides, respectively. Let h_L denotes the optical power gain of channel at the distance of L m, and it can be obtained according to Eq. (6) in [11]. We have that $V_{AC\_Rx} = P_{AC\_Rx} \times R \times g$ and $P_{AC\_Rx} = h_L \times P_{AC\_Tx}$. The former equation means that the APD module with conversion gain of $R \times g$ converts the received

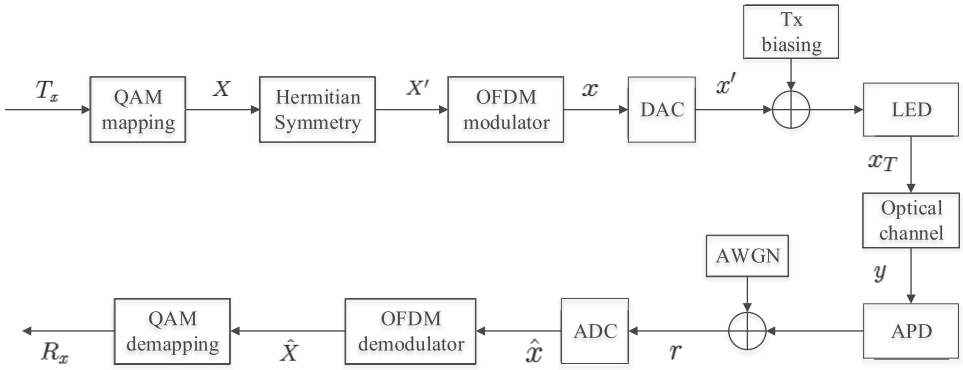

Fig. 3. Block diagram of the DCO-OFDM modulated LED-VLC system.

optical AC signal into electrical signal with voltage of V_{AC_Rx}. Note that the conversion gain $R \times g$ is only determined by ROP. Given a fixed ROP with the fixed $R \times g$ at the receiver side, the transceiver gain G is proportional to the power gain h_L of VLC channel, which can also be regarded as link loss. Explicitly, such proportional relationship can be expressed by:

$$G_{L1}(\text{ROP} = r)/G_{L2}(\text{ROP} = r) = \frac{h_{L1}P_{AC\_Tx}Rg}{V_{AC\_Tx}} \Big/ \frac{h_{L2}P_{AC\_Tx}Rg}{V_{AC\_Tx}} = h_{L1}/h_{L2}, \tag{1}$$

where $G_{L1}(\text{ROP} = r)$ and $G_{L2}(\text{ROP} = r)$ denote the transceiver gains of distances h_{L1} and h_{L2} given ROP=r as transmitting the same signal, respectively. Although the ROPs under certain distance are limited, it can be diversified by focusing lens or optical attenuator.

In order to measure the transceiver voltage gain of adopted APD module, a sinusoidal AC signal with fixed amplitude is transmitted from LED, while the ROP is adjusted by the DC bias V_{dc} that determines the transmitted optical power. Note that the amplitude of AC electrical signal is small enough to avoid the LED's clipping. As for the interference of ambient light, it is relatively small and stable compared with the signal light in the indoor VLC scenario. Therefore, the effect of ambient light on ROP is constant and extremely small, which does not influence the following analysis. After OEC in APD module, we measure the amplitude of received AC electrical signal captured by the oscilloscope, and calculate the transceiver voltage gain G. Fig. 2(b) displays the measured transceiver voltage gain as the function of ROP when the distance between transmitter and receiver is 1 m. It's seen that the gain G remains stable when ROP is less than 20 μW, because APD module is unsaturated for small received optical power. However, the gain G decreases rapidly when ROP is larger than 20 μW, where APD module becomes saturated and its photoelectric gain begins to decrease. Therefore, to enhance the system performance, it is significant to avoid the non-ideal conditions of LED nonlinearity and APD module saturation.

2.3 PAPR Characteristic of OFDM Signal in LED-VLC Systems

The system model of DCO-OFDM modulated indoor LED-VLC is illustrated in Fig. 3. The information bits are mapped into the complex symbols according to M-level quadrature amplitude modulation (M-QAM) scheme, which form the frequency-domain signal vector $\boldsymbol{X} = [X(0), X(1), \ldots, X(N/2-2)]$, where $X(i)$ denotes the electrical QAM symbol, $i = 0, \ldots, N/2-2$, and $N/2-1$ is the number of effective subcarriers transmitting desired signal. As mentioned before, the time-domain signal used to modulate the intensity of the optical carrier must be real in the IM/DD VLC system, which requires the input signal of OFDM modulator to be Hermitian Symmetry. The HS signal $\boldsymbol{X}'$ is constructed as follows:

$$\boldsymbol{X}' = [0, \boldsymbol{X}, \underbrace{0, 0, \ldots, 0}_{N(L-1)/2}, 0, \underbrace{0, 0, \ldots, 0}_{N(L-1)/2}, \boldsymbol{X}^*], \tag{2}$$

where $\boldsymbol{X}^*$ denotes the element-wise conjugate symmetry of $\boldsymbol{X}$. Signal $\boldsymbol{X}'$ contains N(L − 1) padding zeros for L-times over-sampling. It has shown that $L = 4$ is sufficient to capture signal peaks and calculate PAPR accurately [12]. Then $\boldsymbol{X}'$ is send to the OFDM modulator. Let $\boldsymbol{x} = [x(0), \ldots, x(NL-1)]$ denotes the time-domain OFDM symbol output from the OFDM modulator. The n-th element $x(n)$ is given by:

$$x(n) = \frac{1}{\sqrt{NL}} \sum_{m=0}^{NL-1} X'(m) exp\left(\frac{2\pi mn}{NL}\right), \quad 0 \le n \le NL-1, \tag{3}$$

where $X'(m)$ and NL denote the m-th element and the length of vector $\boldsymbol{X}'$, respectively. An OFDM frame is defined as a cluster of U time-domain OFDM symbols whose element is given by Eq. (3). Thus the PAPR of electrical signals within one OFDM frame is defined as

$$PAPR \triangleq \frac{\max\limits_{0 \le n \le UNL-1} |x(n)|^2}{E[|x(n)|^2]}, \tag{4}$$

where $E[\cdot]$ denotes the expectation, the numerator is the peak electrical power and the denominator is the average electrical power of an OFDM frame. Note that the time-domain electrical signal output from OFDM modulator is obtained by superimposing signals of different subcarriers. The peak power of OFDM signal is larger than that of single carrier modulation with the same average power, especially when the instantaneous signal peaks of different subcarriers align at the same time. Therefore, the OFDM signal usually has high PAPR. In the following analysis, we apply the metrics of both cumulative distribution function (CDF) and complementary cumulative distribution function (CCDF) to evaluate the PAPR performance [12], where the CCDF of PAPR is defined as the probability of PAPR being greater than a given reference value.

For the time-domain electrical signal $x(n)$ output from OFDM modulator with large IFFT size, it approximately follows the Gaussian distribution according to the Central Limit Theorem. It has been verified in [12] that the number of sub-carriers as small as 64 is sufficient to approximate the Gaussian distribution. Different from the OFDM complex symbol in RF, whose real and imaginary parts are independent Gaussian variables and the electrical power follows a chi-square distribution with two degrees of freedom (exponential distribution) [13], O-OFDM symbol $x(n)$ is a real value due to the Hermitian Symmetry in IFFT. Thus the instantaneous electrical power of O-OFDM signal obeys a chi-square distribution with one degree of freedom. The CDF of electrical power $|x(n)|^2$ is given by:

$$F(x, 1) = Pr\{P(n) \le x\} = \frac{\gamma(\frac{1}{2}, \frac{x}{2})}{\Gamma(\frac{1}{2})}, \tag{5}$$

where 1 is the degree of freedom of chi-square distribution, $\gamma(s, t)$ denotes the lower incomplete Gamma function. The random variable $|x(n)|^2$ with the normalized average power is supposed to be independent of each other, then CCDF of PAPR for one OFDM frame can be written as

$$Pr(PAPR > x) = 1 - F(x, 1)^{UNL} = 1 - \left(\frac{\gamma(\frac{1}{2}, \frac{x}{2})}{\Gamma(\frac{1}{2})}\right)^{UNL}. \tag{6}$$

Figure 4 illustrates the CCDF as a function of PAPR for OFDM 16-QAM electrical signals. The simulation results of OFDM with and without HS are in good agreement with the theoretical analysis in Eq. (6) and Eq. (14) in [14], respectively. Furthermore, it is shown that the PAPR of OFDM signal with HS is usually larger than that of OFDM without HS. That is because the conjugate symmetry increases the probability of phase coincidence, leading to the large signal peak and high PAPR. In the LED-VLC system based on DCO-OFDM, the signal with high PAPR is prone to work outside the limited linear range of LED source, which would introduce nonlinear distortions. Hence finding proper transmission parameters such as V_{pp} and V_{dc} is imperative.

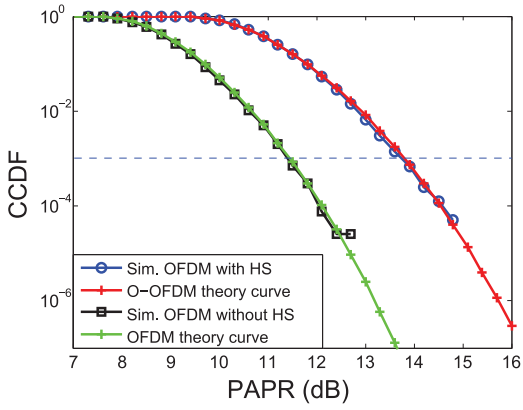

Fig. 4. Theoretical and simulation CCDF of OFDM 16QAM electrical signal with $L = 1$, $U = 5$ and $N = 512$.

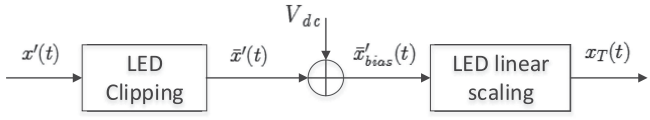

Fig. 5. The equivalent process of electrical-to-optical signal conversion at LED transmitter.

3. Optimal Transmission Based on Maximizing SNDR

3.1 Problem Formulation

LEDs' EOC process can be modeled as the linear scaling followed by the clipping of input signals as illustrated in Section 3. In a LED-VLC system based on DCO-OFDM, before the analog signals are injected into LEDs, a DC bias should be added to ensure the non-negativity of transmitted signal and utilize the linear dynamic range of LEDs effectively. The equivalent process of converting electrical signal into optical one can be modeled in Fig. 5, where the DC bias module is placed after the LED clipping. Such equivalent model will facilitate the following analysis applying Bussgang theorem, which requires the mean value of signals to be clipped to be zero.

The time-domain symbol $x'(t)$ at time t is approximated as a Gaussian random variable according to the Central Limit Theorem, whose mean value and variance are 0 and $\sigma_{x'}^2$, respectively. Then $x'(t)$ is double-side clipped at different bottom and top levels, ε_{bottom} and ε_{top}, where $\varepsilon_{bottom} = U_b - V_{dc}$, $\varepsilon_{top} = U_t - V_{dc}$. As mentioned before, U_b and U_t correspond to the turn-on voltage and the allowable peak voltage, respectively. Let $\lambda_b \triangleq \varepsilon_{bottom}/\sigma_{x'}$ and $\lambda_t \triangleq \varepsilon_{top}/\sigma_{x'}$ denote the normalized bottom and top clipping levels, respectively.

In Fig. 5, $\bar{x}'(t)$ and $\Delta x'(t)$ denote the signal after LED's clipping and the clipped part, respectively. According to Bussgang theorem [15], $\bar{x}'(t)$ can be decomposed into an attenuation term and an uncorrelated non-Gaussian noise term as below:

$$\bar{x}'(t) = x'(t) - \Delta x'(t) = A\,x'(t) + n_c(t), \tag{7}$$

where A is the attenuation factor, which is expressed as [16]:

$$A = Q(\lambda_b) - Q(\lambda_t). \tag{8}$$

According to the probability density function of $\bar{x}'(t)$ [16], $E\{\bar{x}'(t)\}$ and $E\{\bar{x}'^2(t)\}$ are calculated as

$$E\{\bar{x}'(t)\} = \sigma_{x'}[\phi(\lambda_b) - \phi(\lambda_t) + \lambda_b(1 - Q(\lambda_b)) + \lambda_t Q(\lambda_t)], \tag{9}$$

$$E\{\bar{x}'^2(t)\} = \sigma_{x'}^2[Q(\lambda_b) - Q(\lambda_t) - \lambda_t\phi(\lambda_t) + \lambda_b\phi(\lambda_b) + \lambda_b^2(1 - Q(\lambda_b)) + \lambda_t^2 Q(\lambda_t)], \tag{10}$$

where $Q(\cdot)$ and $\Phi(\cdot)$ are the CCDF and probability density function (PDF) of standard normal distribution, respectively. Because the original time-domain signal $x'(t)$ and the clipping noise $n_c(t)$ are independent to each other, Eq. (11) can be obtained according to Eq. (7). Note that the mean value of clipped signal $\bar{x}'(t)$ is equal to that of the noise $n_c(t)$. It's obvious to derive Eq. (12) from Eqs. (9) and (10). Then the variance of the clipping noise can be obtained in (13).

$$E\{\bar{x}'^2(t)\} = A^2\sigma_{x'}^2 + E\{n_c^2\}. \tag{11}$$

$$E\{\bar{x}'^2(t)\} - E^2\{\bar{x}'(t)\} = A^2\sigma_{x'}^2 + E\{n_c^2\} - E^2\{n_c\} = A^2\sigma_{x'}^2 + \sigma_{clip}^2. \tag{12}$$

$$\sigma_{clip}^2 = E\{\bar{x}'^2(t)\} - E^2\{\bar{x}'(t)\} - A^2\sigma_{x'}^2. \tag{13}$$

The clipped signal added by DC bias $\bar{x}'_{bias}$ is given by $\bar{x}'(t) + V_{dc}$. As stated before, LED could be modeled as a linear scaling with double-sides clipping. So the transmitted optical signal $x_T(t)$ can be expressed by:

$$x_T(t) = k(\bar{x}'(t) + V_{dc}) + b = kA\,x' + kn_c + kV_{dc} + b, \tag{14}$$

where k denotes the LED's EOC gain. At the receiver end, APD module filters out the optical DC component and converts the received optical signal $y(t)$ into the electrical AC signal $r(t)$, which is written by:

$$r(t) = Rgh_L\,k\{A\,x'(t) + n_c(t)\} + n_{AWGN}(t), \tag{15}$$

where $n_{AWGN}(t)$ denotes the received noise modeled as AWGN. Based on foregoing definition of G, the transceiver voltage gain $G_L(\text{ROP})$ at distance of h_L can be rewritten as:

$$G_L(\text{ROP}) = R \times g \times P_{AC\_Tx} \times h_L / V_{AC\_Tx} = R \times g \times V_{AC\_Tx} \times k \times h_L / V_{AC\_Tx} = R \times g \times h_L \times k. \tag{16}$$

Thus the received electrical AC signal $r(t)$ can be rewritten as:

$$r(t) = G_L\{A\,x'(t) + n_c(t)\} + n_{AWGN}(t). \tag{17}$$

Let $G_1(\text{ROP})$ denotes the experimentally measured G under different ROP given the distance of 1 m. According to the proportional relationship of Eq. (1), the gain $G_L(\text{ROP})$ can be obtained by:

$$G_L(\text{ROP} = r) = (h_L/h_1) \times G_1(\text{ROP} = r). \tag{18}$$

Therefore, the electrical SNDR is defined as

$$SNDR = \frac{G_L^2(\text{ROP})A^2\sigma_{x'}^2}{G_L^2(\text{ROP})\sigma_{clip}^2 + \sigma_{AWGN}^2}. \tag{19}$$

In this paper, the power of time-domain OFDM electrical signal $x(n)$ is normalized. The average power of continuous signal $x'(t)$ is changed by adjusting V_{pp} at the transmitter. Given the adjustable V_{pp} and the fixed PAPR, the peak power P_{max} and the average power P_{ave} of OFDM continuous electrical signal $x'(t)$ are given by:

$$P_{max} = \frac{1}{4}V_{pp}^2, \tag{20}$$

$$\sigma_{x'}^2 = P_{ave} = \frac{P_{max}}{PAPR} = \frac{V_{pp}^2}{4 \times PAPR}. \tag{21}$$

According to the mathematical expressions of average power, transceiver voltage gain and clipping noise in Eq. (21), (18) and (13), respectively, SNDR can be rewritten as:

$$SNDR(V_{dc}, V_{pp}) = \frac{\frac{(h_L V_{pp})^2}{(2h_1)^2 PAPR} G_1^2(\text{ROP})\left[Q\left(\frac{2(U_b - V_{dc})sqrt(PAPR)}{Vpp}\right) - Q\left(\frac{2(U_t - V_{dc})sqrt(PAPR)}{V_{pp}}\right)\right]^2}{\left(\frac{h_L}{h_1}\right)^2 G_1^2(\text{ROP})\sigma_{clip}^2(V_{dc}, V_{pp}) + \sigma_{AWGN}^2}, \tag{22}$$

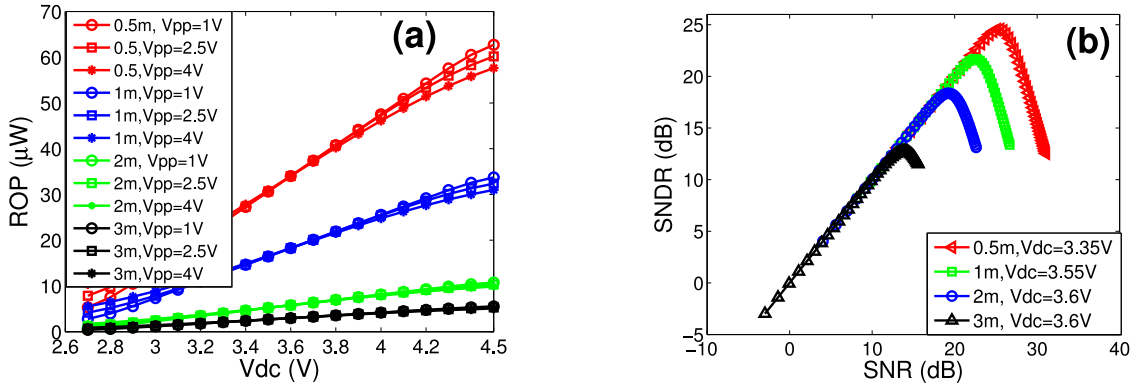

Fig. 6. (a) ROP as a function of V_{dc} under different V_{pp}. It confirms V_{dc} mainly determines ROP. (b) SNDR as a function of SNR. It increases with SNR at first and then declines.

where ROP is mainly determined by V_{dc} as shown in Fig. 6(a) and $\sigma^2_{clip}(V_{dc}, V_{pp})$ can be obtained according to Eq. (9), (10) and (21). It's seen that SNDR is nonlinearly correlative to V_{dc}, V_{pp} as well as APD module saturation, and the received noise. Note that the dominated noise in the system is the sum of thermal noise coming from the resistor of the transimpedance amplifier (TIA), and shot noise, which is due to the ambient light as well as the large avalanche gain of APD. The received noise is independent of the transmitted signal [17] [18]. Consequently, the received noise is a real-valued additive white Gaussian noise (AWGN) with zero mean. When V_{pp} is small enough, the increment of V_{pp} improves the power of electrical AC signal along with the SNDR. However, the overlarge V_{pp} degrades SNDR due to the LED's nonlinear clipping. Furthermore, the overlarge V_{dc} leads to the increment of ROP along with the saturation of APD, which decreases both the transceiver voltage gain G and SNDR. Hence, in the presence of LED clipping and APD module saturation, the optimal transmission parameters, V_{dc} and V_{pp}, need to be studied in order to maximize the SNDR. Note that the DC bias V_{dc} of the adopted LED is bounded by the turn on voltage of 2.7 V as well as the largest permissible voltage of 4.5 V. Consider a reasonable value region of V_{pp} that locates between 0.5 V and 5 V to increase signal power and avoid extremely LED clipping simultaneously. Given the feasible set of V_{dc} and V_{pp}, the SNDR maximization problem can be written as:

$$\begin{aligned} \max_{V_{dc}, V_{pp}} \quad & SNDR(V_{dc}, V_{pp}), \\ s.t. \quad & 2.7 \leqslant V_{dc} \leqslant 4.5, \\ & 0.5 \leqslant V_{pp} \leqslant 5. \end{aligned} \tag{23}$$

3.2 SQP Algorithm

Note that the optimization problem described by Eq. (23) is a complicated non-convex problem, where the explicit expressions of optimal solutions of V_{dc} and V_{pp} are not easy to be obtained. One of the most effective methods for nonlinear optimization problem is to generate steps by solving a series of quadratic subproblems [19], which is powerful for small or large problems with significant nonlinearities. In this paper, we apply this sequential quadratic programming (SQP) algorithm to find the numerical solutions of V_{dc} and V_{pp}. SQP algorithm outputs the final solution once the algorithm converges to optimal point or the number of iteration exceeds the pre-determined maximum step. Note that the initial point is crucial for the convergence of the SQP algorithm. Based on the P-V characteristic of LED, we adopt the medians of the range of V_{dc} and V_{pp} as the initial values, in order to provide the large linear region of LED and the sufficient signal power with small LED clipping. According to the Theorem 18.4 in [19], the sequential steps generated by SQP algorithm converge quadratically to the optimal point when the initial V_{dc} and V_{pp} are close sufficiently to the optimal ones. Hence the adopted SQP algorithm with appropriate initial points can choose the optimal

TABLE 1
Parameters for Simulations and Experiments

V_{DC}	V_{PP}	IFFT Point	Modulation Order	PAPR
2.7V-4.5V	0.5V-5V	128	16QAM	12dB

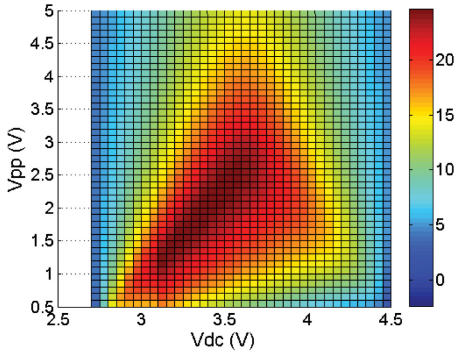

(a) $0.5m$ without lens. Optimal parameters (V_{dc}, V_{pp}): (3.35, 1.9), (3.4, 2.1), (3.45, 2.2). Maximum $SNDR = 24.55dB$

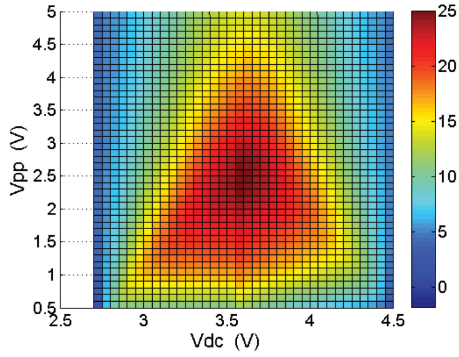

(b) $1m$ without lens. Optimal parameter (V_{dc}, V_{pp}): (3.55, 2.6). Maximum $SNDR = 21.69dB$

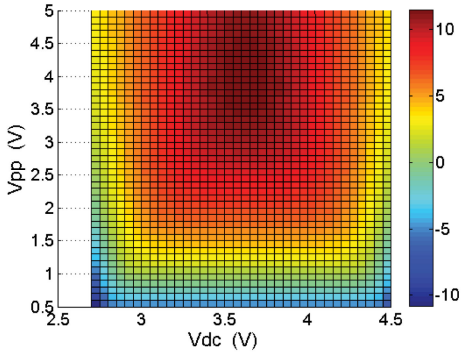

(c) $3m$ without lens. Optimal parameter (V_{dc}, V_{pp}): (3.6, 3.6). Maximum $SNDR = 12.77dB$

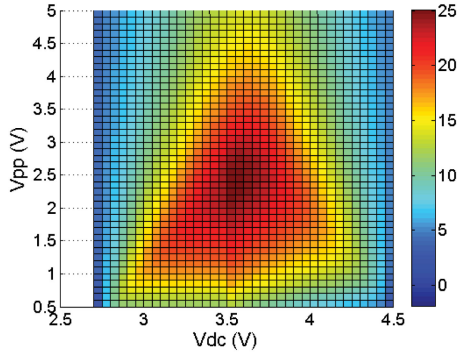

(d) $3m$ with lens. Optimal parameter (V_{dc}, V_{pp}): (3.55, 2.5). Maximum $SNDR = 25.03dB$

Fig. 7. Simulated SNDR performance as a function of V_{dc} and V_{pp} at different transmission distances.

transmission parameters and optimize SNDR quickly when the position of the receiver changes, which is capable of satisfying the delay and performance requirement of practical LED-VLC system.

4. Simulation and Experimental Results and Discussions

4.1 Simulation and Experimental Results for SNDR

The parameters for both simulation and experiments are listed in Table 1, where the variables V_{DC} and V_{PP} denote the feasible sets of V_{dc} and V_{pp}, respectively. As we can see in Fig. 6(b), *SNDR* displays total different trend from the traditional *SNR* due to the nonlinear distortions. Considering the distances h_L of 0.5 m, 1 m and 3 m, we show the SNDR as the function of V_{dc} and V_{pp} in Fig. 7. In the case of 0.5 m, the ROP exceeds 20 μW when V_{dc} is larger than 3.1 V, which means that the APD module intends to be saturated according to the characteristic of adopted APD module as shown in Fig. 2(b). It can be seen from Fig. 7(a) that the optimal region with larger SNDR exhibits to be striped. That is because both large V_{pp} and V_{dc} lead to the saturation of APD module and thus

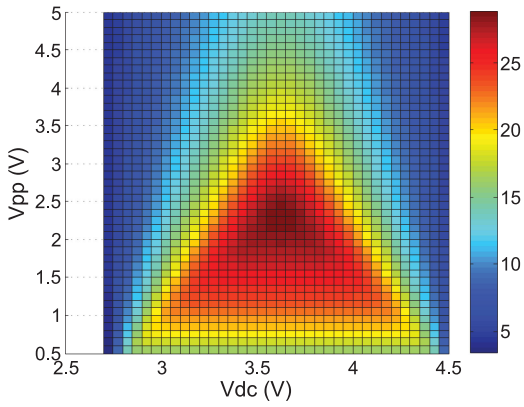

Fig. 8. Simulated SNDR performance as a function of V_{dc} and V_{pp} at 0.5 m without lens. Assume that APD module has excellent properties. Optimal parameter (V_{dc}, V_{pp}): (3.6, 2.5).

the decrement of gain G, even though the signal power is improved at the same time. On the other hand, both small V_{pp} and V_{dc} provide a suitable ROP to avoid the APD module saturation and then have high gain G, even though the signal power is smaller than that of large V_{pp}. Furthermore, in the practical system with APD module working in the saturated status, the simulation results show that the decrement of both V_{dc} and V_{pp} can keep the same SNDR with the large V_{dc} and V_{pp} while decreasing the transmitted power and thus saving energy consumption.

In the case of 1 m where the ROP (4 μW–30 μW) provides a good APD module working status of large gain G, the best V_{dc} and V_{pp} will locate near the median of V_{DC} and V_{PP} as shown in Fig. 7(b). That is because the SNDR performance is mainly up to the clipping noise at transmitter side when G is large enough. As shown in the P-V characteristic of the adopted LED in Fig. 2(a), the medians of V_{DC} and V_{PP} provide a large linear dynamic region and prevent the transmitted signal from being clipped, respectively. In the case of 3 m where the large link loss leads to the decrement of ROP (less than 4 μW), SNDR performance degrades greatly due to the loss of optical AC power, even though the transceiver voltage gain G is large at this situation. It can be seen from Fig. 7(c) that the optimal V_{dc} is still around the median of V_{DC}, where LED works at the linear range. But the optimal V_{pp} is larger than the median value of V_{PP}, because more signal power is needed to improve the SNDR even though the clipping noise increases meanwhile. It can be concluded that with the increment of transmission distance, the large link loss leads to the decrement of ROP and thus the unsaturated status of APD module, where more V_{pp} is needed to enhance the signal power along with the SNDR. In the case of large transmission distance, increasing ROP by the lens could improve SNDR effectively rather than increasing V_{dc} and V_{pp}. It can be confirmed in Fig. 7(c) and (d), where the maximum SNDR is increased from 12 dB to 25 dB compared with the case of 3 m without lens in Fig. 7(c).

Suppose that APD module has a constant conversion gain and the saturation characteristic is ignored. Then the SNDR performance relies mainly on the LED clipping noise. Fig. 8 shows the simulation results of SNDR at the distance of 0.5 m. It can be seen that the optimal V_{pp} and V_{dc} are close to medians of V_{PP} and V_{DC}, respectively, because such transmission parameters provide both large linear working range and signal power with small LED clipping.

Figure 9(a) shows SNDR as the function of V_{pp} considering a specific set of transmission distance along with the corresponding optimal V_{dc}. Compared with [10], our contributions lie in the following two aspects. One is that the APD saturation characteristic is considered. The other is that V_{dc} is proved to be an important parameter affecting SNDR except for V_{pp}. It's seen that given a specific transmission distance and optimal V_{dc}, SNDR first increases with the V_{pp}, and then decreases. That is because large V_{pp} will lead to worse LED clipping and thus the decrement of SNDR, even though it provides more signal power. Furthermore, for the transmission distance of 0.5 m, the optimal V_{pp} of $V_{dc} = 3.55\ V$ is larger than that of $V_{dc} = 3.1\ V$, which is consistent to the results in Fig. 7(a). That is because large V_{dc} and V_{pp} improve the signal power but saturate the APD module, while small ones

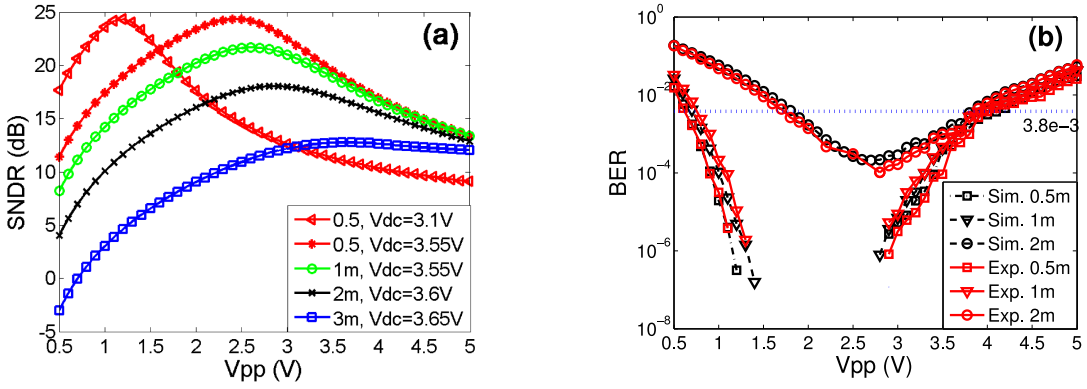

Fig. 9. (a) Simulation SNDR performance as a function of V_{pp} at different transmission distances. (b) Simulation and experimental BER performance as a function of V_{pp} at different transmission distances.

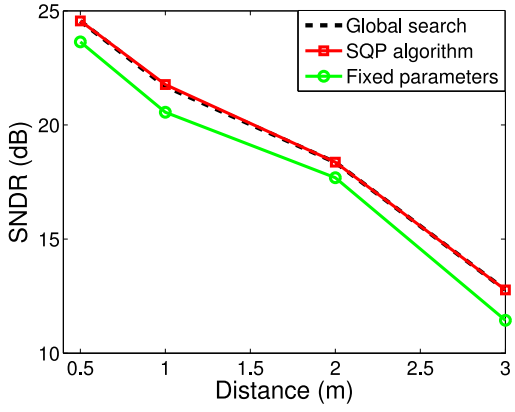

Fig. 10. SNDR performance comparison with different algorithms for transmission parameters.

avoid saturation status and thus improve gain G, even though the signal power is small. Fig. 9(b) shows both the simulation and the experiment results of BER as the function of V_{pp}. It's seen that the experimental BER values agree with the simulation ones, which demonstrates the correctness of theoretical analysis in this paper. The BER first decreases with V_{pp} and then increases, which corresponds to the simulation results in Fig. 9(a). In addition, the optimal V_{pp} increases with the increment of transmission distance. That is because a small V_{pp} is desired to avoid LED clipping and APD saturation at small distance, while large V_{pp} is necessary to provide more signal power at large distance even though the clipping noise is large, which is consistent to the previous analysis for Fig. 7 and Fig. 9(a).

4.2 Simulation Results for SQP Algorithm

In this paper, the SQP algorithm is applied to solve the non-convex optimization problem as shown in Eq. (23). We investigate the SNDR performances using global search, SQP algorithm and fixed parameters in Fig. 10. In addition, the SNDR updates during the iteration process of SQP are shown in Fig. 11. Note that the global search algorithm finds the optimal V_{dc} and V_{pp} with step size of 0.05 V, and the medians of V_{DC} and V_{PP} are adopted as the fixed parameters. It has been shown that such fixed V_{dc} and V_{pp} obtain good SNDR performances at different transmission distances in the previous results. It's seen that both SQP and global search have the close optimal SNDRs and about 1 dB gain in terms of SNDR compared with the fixed parameters algorithm. The mean square

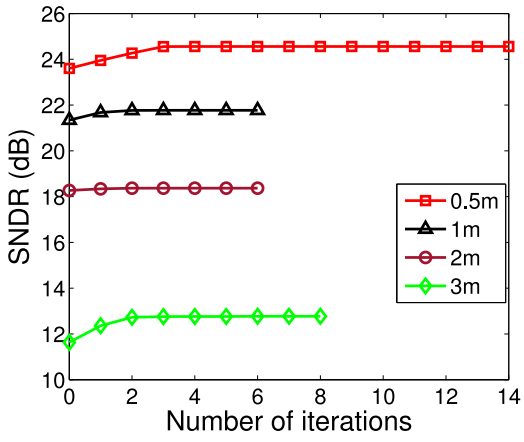

Fig. 11. SNDR updates in the iteration process of SQP.

TABLE 2
Comparison of Average Computing Time Under Different Algorithms

Global search	Step size (V_{dc}, V_{pp})	Mean computing time
(1)	0.05V / 0.05V	0.2705s
(2)	0.05V / 0.1V	0.1381s
SQP algorithm	Maximum iteration step	Mean computing time
(1)	8	0.02719s
(2)	5	0.00948s

error of optimal SNDR between SQP and the global search algorithm is 0.0016. From Fig. 11, it's seen that SNDR intends to be stable within 4 steps, which illustrates that SQP algorithm converges to the optimal point quickly.

Usually, the practical system requires a small delay of updating optimal transmission parameters when the position of the receiver changes. In Table 2, we compare the average computation times of global search and SQP in terms of computation time measured in the MATLAB environment. Two step sizes are considered for the global search: one is (0.05 V, 0.05 V), and the other is (0.05 V, 0.1 V). Two maximum iteration steps are considered for SQP algorithm: 5 and 8. It's shown that the computation time of global search is about ten times than that of SQP. Even though the increment of step size will decrease the computation time of global search, there is no doubt that the optimal SNDR found by large step is smaller than that of small step. However, the optimal SNDRs of SQP with maximum iteration steps of 5 and 8 are close to each other. It means that a suitable maximum step of SQP could be selected for a practical VLC system, which obtains the globally optimal SNDR with the smallest computation time. The performance of the SQP algorithm supports that if the ROP and the link gain h_L of the receiver can be fed back through the RF uplink as shown in Fig. 1, the optimal transmission parameters can be obtained rapidly and effectively to achieve the optimal transmission all the time.

5. Conclusion

In this paper, we propose to optimize the transmission parameters V_{pp} and V_{dc} based on maximizing SNDR in the presence of LED's clipping and APD module saturation. The analytic expression of

SNDR and a SQP algorithm are presented to solve the problem. To the best of our knowledge, it is the first time to jointly reduce the nonlinear distortions caused by both LED clipping and APD module saturation via both simulations and experiments. The results indicate that the optimal transmission parameters V_{pp} and V_{dc} lie around the median of V_{PP} and V_{DC} when the suitable ROP provides enough signal power and unsaturated status of APD module. It is interesting to observe that when the APD module is saturated, the smaller V_{dc} and V_{pp} achieve the best SNDR performance with small energy consumption. However, when ROP is extremely small, the optimal V_{pp} should be increased to provide more signal power even working in the LED's nonlinear range. These optimal parameters can be obtained accurately and efficiently by applying SQP algorithm to solve the SNDR maximization problem. Moreover once the location of the user changes, the optimal performance can still be guaranteed through updating the transmission parameters by SQP algorithm. It's believed that the comprehensive studies of the distortions caused by devices, the formulation of SNDR and the SQP algorithm provide a significant guidance to achieve the optimal transmission performance in the classical LED-VLC systems depicted in Fig. 1.

References

[1] H. Elgala, R. Mesleh, and H. Haas, "Indoor optical wireless communication: potential and state-of-the-art," *IEEE Commun. Mag.*, vol. 49, no. 9, pp. 56–62, Sep. 2011.
[2] "Characteristics and use of Si APD," *Hamamatsu Photonics*, May 2004.
[3] H. Elgala, R. Mesleh, and H. Haas, "Practical considerations for indoor wireless optical system implementation using OFDM," in *Proc. IEEE 10th Int. Conf. Telecommun., Zagreb, Croatia*, Jun. 2009, pp. 25–29.
[4] J. Armstrong, "OFDM for optical communications," *J. Lightw. Technol.*, vol. 27, no. 3, pp. 189–204, Feb. 2009.
[5] J. M. Kahn and J. R. Barry, "Wireless infrared communications," *Proc. IEEE*, vol. 85, no. 2, pp. 265–298, Feb. 1997.
[6] J. Armstrong and A. Lowery, "Power efficient optical OFDM," *Electron. Lett.*, vol. 42, no. 6, pp. 370–372, Mar. 2006.
[7] J. Armstrong and B. J. Schmidt, "Comparison of asymmetrically clipped optical OFDM and DC-biased optical OFDM in AWGN," *IEEE Commun. Lett.*, vol. 12, no. 5, pp. 343–345, May 2008.
[8] H. Elgala, R. Mesleh, and H. Haas, "Impact of LED nonlinearities on optical wireless OFDM systems," in *Proc. IEEE 21st Int. Symp. PIMRC*, Sep. 2010, pp. 634–638.
[9] H. Elgala, R. Mesleh, and H. Haas, "A study of LED nonlinearity effects on optical wireless transmission using OFDM," in *Proc. 6th IEEE Int. Conf. Wireless Opt. Commun. Netw.*, Apr. 2009, pp. 1–5.
[10] S. Zhao, S. Cai, K. Kang, and H. Qian, "Optimal transmission power in a nonlinear VLC system," in *Proc. IEEE Global Conf. Signal Inf. Process.*, Dec. 2015, pp. 1180–1184.
[11] T. Komine and M. Nakagawa, "Fundamental analysis for visible-light communication system using LED lights," *IEEE Trans. Consum. Electron.*, vol. 50, no. 1, pp. 100–107, Feb. 2004.
[12] Y. Rahmatallah and S. Mohan, "Peak-to-average power ratio reduction in OFDM systems: A survey and taxonomy," *IEEE Commun. Surveys Tuts.*, vol. 15, no. 4, pp. 1567–1592, Mar. 2013.
[13] M. Park, H. Jun, J. Cho, N. Cho, D. Hong, and C. Kang, "PAPR reduction in OFDM transmission using Hadamard transform," in *Proc. Int. Conf. Commun.*, Jun. 2000, vol. 1, pp. 430–433.
[14] T. Jiang and Y. Wu, "An overview: Peak-to-average power ratio reduction techniques for ofdm signals," *IEEE Trans. Broadcast.*, vol. 54, no. 2, pp. 257–268, Feb. 2008.
[15] J. J. Bussgang, "Crosscorrelation functions of amplitude-distorted Gaussian signals," *Res. Laboratory Electron., Massachusetts Inst. Technol.*, 1952.
[16] S. Dimitrov, S. Sinanovic, and H. Haas, "Clipping noise in OFDM-based optical wireless communication systems," *IEEE Trans. Commun.*, vol. 60, no. 4, pp. 1072–1081, Apr. 2012.
[17] B. Ghimire and H. Haas, "Self-organising interference coordination in optical wireless networks," *Eur. J. Wireless Commun. Netw.*, vol. 2012, no. 1, pp. 131–145, Dec. 2012.
[18] K. Wang, A. Nirmalathas, C. Lim, and E. Skafidas, "Impact of background light induced shot noise in high-speed full-duplex indoor optical wireless communication systems," *Opt. Exp.*, vol. 19, no. 22, pp. 21 321–21 332, 2011.
[19] S. Wright and J. Nocedal, "Numerical optimization," *Springer Sci.*, vol. 35, no. 67–68, pp. 526–573, 1999.